RT–PCR and real-time PCR

Human lens cells were obtained with informed consent from the anterior capsules of patients with senile cataracts. Human lens epithelial cell line (LEC) was established by infecting lens epithelial cells with Adeno 12-SV40 hybrid virus[26], and was previously described[27]. RNA was prepared by the acid phenol-guanidine thiocyanate method. RNA from human liver and thymus was purchased from Biochain Institute and BD Biosciences Clontech, respectively. The human DLAD mRNA[8] was detected by RT–PCR using primers 5′-GTGGCATCTGCATAACTTTC and 5′-GGTCTCCAATACATGTCCAG. For real-time PCR, RNA was treated with RNase-free DNase I (Invitrogen), and reverse-transcribed using Superscript II reverse-transcriptase (Invitrogen). The real-time PCR was carried out using a LightCycler (Roche Diagnostics) according to the instructions provided by the manufacturer. Primers for the mouse DLAD mRNA were: 5′-CCAGTTCATGGCTATGAG TAC and 5′-TTAGGTCTCCAATGCAGGTCCAGCGATTTG. As a control, the expression of the mouse β-actin gene was detected using primers 5′-TGTGATGGTGGGAATGGGT CAG and 5′-TTTGATGTCACGCACGATTTCC. The level of specific mRNA was quantified at the point where the LightCycler System detected the upstroke of the exponential phase of PCR accumulation, and normalized to the level of β-actin in each sample.

Assay for acid DNase

The lenses were homogenized in lysis buffer (10 mM Tris–HCl (pH 7.5), 1 M NaCl, and 1 mM *p*APMSF). After removing the cell by centrifugation, the supernatant was dialysed against 50 mM citrate buffer (pH 5.0) containing 1 mM EDTA, and the acid DNase activity was measured as described[9]. In brief, plasmid DNA (2.0 μg) was mixed with the sample in 120 μl of the reaction mixture (50 mM MOPS-NaOH buffer (pH 5.9) containing 10 mM EDTA). After incubation at 37 °C for 3 h, the mixture was treated with phenol-chloroform, and the DNA was recovered by EtOH precipitation.

Histochemical and electron microscopic analysis of eye lens

For histological analysis, mouse lens at 6 weeks of age was fixed in 4% paraformaldehyde/4% sucrose in 0.1 M phosphate buffer (pH 7.2), embedded in paraffin, and sectioned at 4 μm. The sections were treated for 10 min with 1 N HCl at 60 °C, and subjected to Feulgen staining. To detect mitochondrial ATP synthase, the sections were incubated overnight at 4 °C with rabbit antibody against subunit β of mitochondrial ATP synthase[28], followed by the Cy3-coupled goat anti-rabbit IgG, F(ab')2 fragment (Jackson ImmunoResearch Lab.). For electron microscopy, the lenses from 6-week-old mice were fixed with 4% glutaraldehyde in 0.1 M phosphate buffer (pH 7.2), post-fixed with 1% OsO_4 at 4 °C for 2 h, and embedded in Epon 812. Sections (80 nm) were prepared with an ultramicrotome (Reichert Ultracut N), stained with lead citrate and uranyl acetate, and observed with an H-7100 electron microscope (Hitachi High-Technologies Co.).

Electroretinograms

ERGs were obtained as described previously[29]. In brief, mice were dark-adapted for more than 12 h and anaesthetized by a subcutaneous injection of xylazine and ketamine. The cornea was anaesthetized with 0.4% oxybuprocaine, and the pupils were dilated with 0.5% tropicamide and 0.5% phenylephrine-HCl. ERGs were recorded from the corneal surface of one eye using chlorided silver wire loops. The luminance of the unattenuated light stimulus was 3.7 log(cd m^{-2}) on the surface of the eye, and different neutral-density filters were used to serially reduce the stimulus intensities. Responses were amplified at a 10,000 gain with a band-pass frequency setting of 0.08–1,000 Hz (Nihon Kohden, VC-11). Single-flash stimulus intensities were increased from 1.8 log(cd m^{-2}) to 3.7 (log cd m^{-2}), and divided into 4 steps. Ten responses were averaged with an averager (Nihon Kohden, LEG-1000).

Received 28 March; accepted 4 July 2003; doi:10.1038/nature01895.

1. McAvoy, J. W., Chamberlain, C. G., de Iongh, R. U., Hales, A. M. & Lovicu, F. J. Lens development. *Eye* **13,** 425–437 (1999).
2. Grainger, R. M., Henry, J. J., Saha, M. S. & Servetnick, M. Recent progress on the mechanisms of embryonic lens formation. *Eye* **6,** 117–122 (1992).
3. Piatigorsky, J. Lens differentiation in vertebrates. A review of cellular and molecular features. *Differentiation* **19,** 134–153 (1981).
4. Wistow, G. J. & Piatigorsky, J. Lens crystallins: The evolution and expression of proteins for a highly specialized tissue. *Annu. Rev. Biochem.* **57,** 479–504 (1988).
5. Bassnett, S. Lens organelle degradation. *Exp. Eye Res.* **74,** 1–6 (2002).
6. Bassnett, S. & Mataic, D. Chromatin degradation in differentiating fiber cells of the eye lens. *J. Cell Biol.* **137,** 37–49 (1997).
7. Shiokawa, D. & Tanuma, S. DLAD, a novel mammalian divalent cation-independent endonuclease with homology to DNase II. *Nucleic Acids Res.* **27,** 4083–4089 (1999).
8. Krieser, R. J., MacLea, K. S., Park, J. P. & Eastman, A. The cloning, genomic structure, localization, and expression of human deoxyribonuclease IIβ. *Gene* **269,** 205–216 (2001).
9. Kawane, K. *et al.* Requirement of DNase II for definitive erythropoiesis in the mouse fetal liver. *Science* **292,** 1546–1549 (2001).
10. Krieser, R. J. *et al.* Deoxyribonuclease IIa is required during the phagocytic phase of apoptosis and its loss causes lethality. *Cell Death Differ.* **9,** 956–962 (2002).
11. Kawane, K. *et al.* Impaired thymic development in mouse embryos deficient in apoptotic DNA degradation. *Nature Immunol.* **4,** 138–144 (2003).
12. Nagata, S., Nagase, H., Kawane, K., Mukae, N. & Fukuyama, H. Degradation of chromosomal DNA during apoptosis. *Cell Death Differ.* **10,** 108–116 (2003).
13. Kuwabara, T. & Imaizumi, M. Denucleation process of the lens. *Invest. Ophthalmol. Vis. Sci.* **13,** 973–981 (1974).
14. Torriglia, A. *et al.* L-DNase II, a molecule that links proteases and endonucleases in apoptosis, derives from the ubiquitous serpin leukocyte elastase inhibitor. *Mol. Cell. Biol.* **18,** 3612–3619 (1998).
15. Bernardi, G., (ed. Boyer, P. D.)) *The Enzymes*, 271–287 (Academic, New York, 1971).
16. Wride, M. A. & Sanders, E. J. Nuclear degeneration in the developing lens and its regulation by TNFα. *Exp. Eye Res.* **66,** 371–383 (1998).
17. Dahm, R., Gribbon, C., Quinlan, R. A. & Prescott, A. R. Changes in the nucleolar and coiled body compartments precede lamina and chromatin reorganization during fibre cell denucleation in the bovine lens. *Eur. J. Cell Biol.* **75,** 237–246 (1998).
18. Ishizaki, Y., Jacobson, M. D. & Raff, M. C. A role for caspases in lens fiber differentiation. *J. Cell Biol.* **140,** 153–158 (1998).
19. Chaudun, E. *et al.* DNA strand breakage during physiological apoptosis of the embryonic chick lens: Free 3′ OH end single strand breaks do not accumulate even in the presence of a cation-independent deoxyribonuclease. *J. Cell. Physiol.* **158,** 354–364 (1994).
20. McIlroy, D. *et al.* An auxiliary mode of apoptotic DNA fragmentation provided by phagocytes. *Genes Dev.* **14,** 549–558 (2000).
21. Klionsky, D. J. & Emr, S. D. Autophagy as a regulated pathway of cellular degradation. *Science* **290,** 1717–1721 (2000).
22. Klionsky, D. J. & Ohsumi, Y. Vacuolar import of proteins and organelles from the cytoplasm. *Annu. Rev. Cell Dev. Biol.* **15,** 1–32 (1999).
23. Vrensen, G. F., Graw, J. & De Wolf, A. Nuclear breakdown during terminal differentiation of primary lens fibres in mice: A transmission electron microscopic study. *Exp. Eye Res.* **52,** 647–659 (1991).
24. Laird, P. W. *et al.* Simplified mammalian DNA isolation procedure. *Nucleic Acids Res.* **19,** 4293 (1991).
25. Sambrook, J. & Russell, D. W. *Molecular Cloning: A Laboratory Manual* (Cold Spring Harbor Laboratory, Cold Spring Harbor, New York, 2001).
26. Fleming, T. P., Song, Z. & Andley, U. P. Expression of growth control and differentiation genes in human lens epithelial cells with extended life span. *Invest. Ophthalmol. Vis. Sci.* **39,** 1387–1398 (1998).
27. Imoto, Y. *et al.* Effects of RGD peptides on cells derived from the human eye. *Jpn J. Ophthal.* (in the press).
28. Ezaki, J., Wolfe, L. S. & Kominami, E. Specific delay in the degradation of mitochondrial ATP synthase subunit c in late infantile neuronal ceroid lipofuscinosis is derived from cellular proteolytic dysfunction rather than structural alteration of subunit c. *J. Neurochem.* **67,** 1677–1687 (1996).
29. Masu, M. *et al.* Specific deficit of the ON response in visual transmission by targeted disruption of the mGluR6 gene. *Cell* **80,** 757–765 (1995).

Acknowledgements We thank E. Kominami for providing us with rabbit antibody against the subunit β of mitochondrial ATP synthase. We thank K. Miwa for cloning of mouse DLAD gene, Y. Seto for maintaining the mice, and M. Fujii and M. Harayama for secretarial assistance. This work was supported in part by Grants-in-Aid from the Ministry of Education, Science, Sports, and Culture in Japan.

Competing interests statement The authors declare that they have no competing financial interests.

Correspondence and requests for materials should be addressed to S.N. (nagata@genetic.med.osaka-u.ac.jp).

Determining the position of the cell division plane

Julie C. Canman[1]*, Lisa A. Cameron[1]†, Paul S. Maddox[1]†, Aaron Straight[2], Jennifer S. Tirnauer[2], Timothy J. Mitchison[2], Guowei Fang[3], Tarun M. Kapoor[4] & E. D. Salmon[1]

[1]*University of North Carolina, Department of Biology, 607 Fordham Hall, CB #3280, Chapel Hill, North Carolina 27699-3280, USA*
[2]*Harvard Medical School, Department of Cell Biology, 250 Longwood Avenue, Boston, Massachusetts 02115, USA*
[3]*Stanford University, Department of Biological Sciences, Stanford, California 94305, USA*
[4]*Laboratory of Chemistry and Cell Biology, The Rockefeller University, New York, New York 10021, USA*

* Present address: University of Oregon, Institute of Molecular Biology, 1370 Franklin Blvd., Eugene, Oregon, USA
† These authors contributed equally to this work

Proper positioning of the cell division plane during mitosis is essential for determining the size and position of the two daughter cells—a critical step during development and cell differentiation[1]. A bipolar microtubule array has been proposed to be a minimum requirement for furrow positioning in mammalian cells, with furrows forming at the site of microtubule plus-end overlap between the spindle poles[2–4]. Observations in other species have suggested, however, that this may not be true[5,6]. Here we show, by inducing mammalian tissue cells with

monopolar spindles to enter anaphase[7,8], that furrow formation in cultured mammalian cells does not require a bipolar spindle. Unexpectedly, cytokinesis occurs at high frequency in monopolar cells. Division always occurs at a cortical position distal to the chromosomes. Analysis of microtubules during cytokinesis in cells with monopolar and bipolar spindles shows that a subpopulation of stable microtubules extends past chromosomes and binds to the cell cortex at the site of furrow formation. Our data are consistent with a model in which chromosomes supply microtubules with factors that promote microtubule stability and furrowing.

How microtubules control the positioning of the cell division plane is the subject of much controversy. In current models, microtubules either promote furrowing at the cell equator by means of the overlap zone of microtubules from opposite poles, or restrict furrowing to the cell equator by means of the microtubule asters inhibiting cortical contractility at the cell poles[2–4]. A central tenet of these models is that dividing cells must have bipolar arrays of microtubules.

We used monastrol, an inhibitor of the kinesin Eg5 and centrosome separation[7,8], to test whether a bipolar microtubule array is essential for cytokinesis in mammalian tissue cells. Treatment of PtK1 cells with monastrol resulted in both the formation of monopolar half-spindles with two unseparated centrosomes near one spindle pole (Fig. 1a) and activation of the mitotic spindle checkpoint. To overcome the spindle checkpoint and induce the cytokinetic phase (C-phase)[9] of the cell cycle, cells with monopolar spindles were injected with anti-Mad2 antibodies, Mad2ΔC, or Mad1F10 (refs 10–12). After injection, cells with monopolar spindles entered anaphase in 22 ± 7 min (Fig. 1b, c, and Supplementary Movie 1) and both sister chromatids moved toward the spindle pole ($n = 15$, Fig. 1c and Supplementary Movie 1).

More than 90% of the cells that entered anaphase underwent cytokinesis (14/15, Fig. 1c and Supplementary Movie 1). Furrows formed within 6 ± 2 min, a time that is typical of control cells with bipolar spindles[9]. Monopolar spindles were frequently asymmetric and resembled a 'half-spindle' with all chromosomes on one side of the unseparated centrosomes (Fig. 1a). Likewise, cytokinesis was polarized in these cells: cytokinetic furrows always occurred on the side of the cell facing the chromosomes and not on the side facing the unseparated centrosomes (14/14; Fig. 1c and see below). Furrowing occurred 25 ± 4 μm away from the spindle pole, resulting in the formation of a small anucleate cytoblast (Fig. 1c). These cytokinetic furrows were stable, persisting for at least 3 h after furrow completion and cell respreading. Thus, two opposing microtubule arrays are not essential for cytokinesis in cultured mammalian cells.

In normal cells 'chromosome passenger' proteins, including INCENP, Survivin and Aurora B, translocate along microtubules during anaphase and cytokinesis from the centromeric chromatin to the cell equator[12–15]. An accumulation of passenger proteins at the equator is essential for cytokinesis[16] and is thought to depend on an antiparallel microtubule array[15]. To test whether centromere-associated proteins relocate to the furrow region of cells with monopolar spindles, we examined changes in the localization of INCENP after anaphase onset[12]. Monastrol-treated PtK1 cells with monopolar spindles were fixed either before or after microinjection with Mad2ΔC at the time of furrow initiation. Cells were then immunostained for tubulin, INCENP and DNA. In non-injected cells with monopolar spindles, INCENP localized to the centromeres (data not shown). In monopolar cells induced into anaphase, there was marked accumulation of INCENP at the furrow (Fig. 2). Thus, an overlapping bipolar array of microtubules is not needed to localize INCENP to the furrow region.

As microtubules are essential for furrow positioning[9], we wanted to examine the behaviour of microtubules during cytokinesis in living cells with monopolar spindles. We pretreated cells with monastrol, co-injected fluorescently labelled tubulin and Mad2ΔC, and imaged microtubule dynamics by spinning disk confocal microscopy. At anaphase onset, the microtubules lengthened markedly, growing out towards the cell cortex (Fig. 3a). Although many of these microtubules were highly dynamic, a subset of microtubules were stable and bound to the cell cortex. These stable microtubules were found only on the side of the cell facing the chromosomes. Kymographic analysis indicated that cortical microtubules extending past the chromosomes were four times as stable as microtubules growing towards the side of the cell facing the spindle pole (median lifetime 224 ± 119 s ($n = 115$) at furrow versus

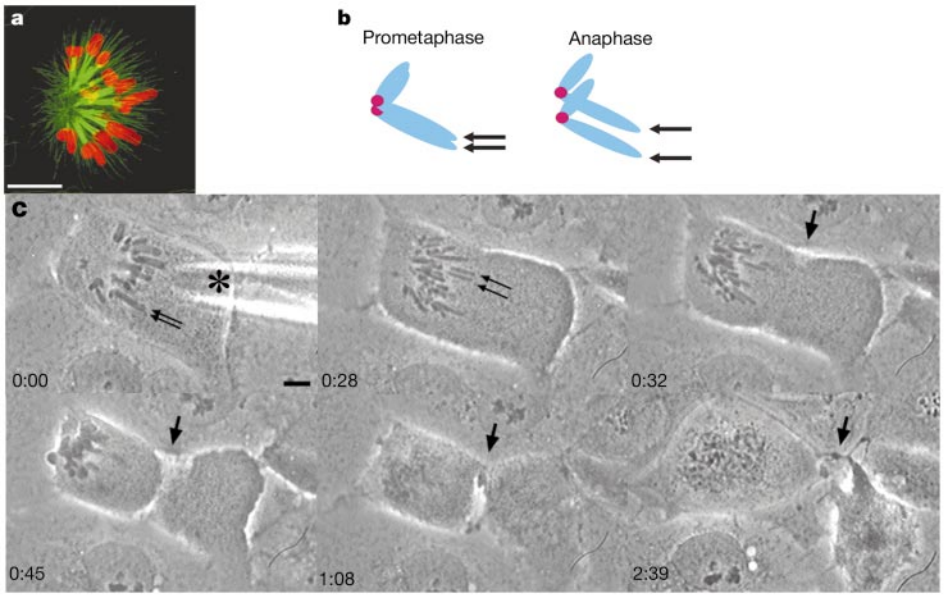

Figure 1 Cytokinesis in cells with monopolar spindles **a**, Monastrol-treated PtK1 cell in prometaphase cell stained for tubulin (green) and DNA (red). **b**, Diagram of anaphase in monastrol with both sister chromatids facing the same spindle pole. **c**, Cytokinesis in a cell induced into anaphase by microinjection of Mad2ΔC. Asterisk indicates injection needle. Small arrows indicate sister separation. Large arrow indicates furrow position. In each frame, time is given in h:min. Scale bars, 5 μm.

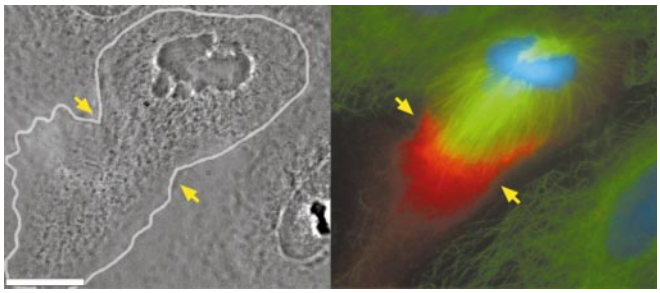

Figure 2 INCENP localizes to furrows in cells with monopolar spindles. Monastrol-treated PtK1 cell injected with Mad2ΔC, recorded through anaphase and furrow onset, and then fixed. Left, phase contrast highlights cell outline (traced in white). Arrows indicate furrow site. Right, the cell was then processed for immunofluorescence of tubulin (green), INCENP (red) and DNA (blue). Scale bar, 10 μm.

64 ± 38 s ($n = 187$) at pole; Fig. 3b, c, and Supplementary Movie 2). This precise correlation between the position of the chromosomes and the appearance of stable microtubules indicates that chromosomes may have a direct role in furrow positioning through microtubules.

To test further this relationship between chromosomes and stable microtubules, we examined the behaviour of microtubules in cells with bipolar spindles injected with labelled tubulin. After anaphase onset, but before furrow onset, we observed a marked polymerization of microtubules toward the cell cortex in the furrow regions as well as in the polar regions (Fig. 3d and Supplementary Movie 3). Kymographic analysis of these movies showed that dynamic microtubules, which populated the polar regions of the cell, did not form stable cortical interactions even if they contacted the cell cortex at the site of furrow formation (median lifetime 60 ± 41 s ($n = 247$); for example, see left aster, bottom equator in Supplementary Movie 3 and Fig. 3e). These microtubules may be acting to suppress furrowing activity in the polar regions of the cell as ectopic furrowing occurs throughout the cell cortex in the absence of microtubules[9,17,18].

In contrast, a stable subpopulation of microtubules was located in the region of the furrow (median lifetime, 123 ± 60 s ($n = 207$); Fig. 3f and Supplementary Movie 3). Notably, these stable microtubules were associated with, or 'passed by', a kinetochore fibre or chromosome for about 75% of the time (87/115 stable microtubules; Fig. 3g, h). Dynamic microtubules could be also seen in the equatorial region; however, these microtubules did not bind the cell cortex. Thus, in cells with bipolar spindles there is also a precise correlation between the localization of the chromosomes and the formation of stable microtubules in both PtK1 cells (Fig. 3f) and in U2OS cells (data not shown). Therefore, cytokinesis in cells with bipolar spindles (Fig. 4b) seems to occur as the sum of two asymmetric monopolar spindles (Fig. 4a): the stable, chromosome-associated microtubules bind the cell cortex at the site of furrow formation, whereas dynamic astral microtubules populate the polar regions.

We have shown that microtubule dynamics are asymmetric within a single cell during cytokinesis, with furrows forming near areas of high numbers of stable microtubule ends. This is seemingly in opposition to studies in *Caenorhabditis elegans*, which concluded that furrow formation is dependent on a reduced microtubule density in the furrow region[19]. It is also possible, however, that a

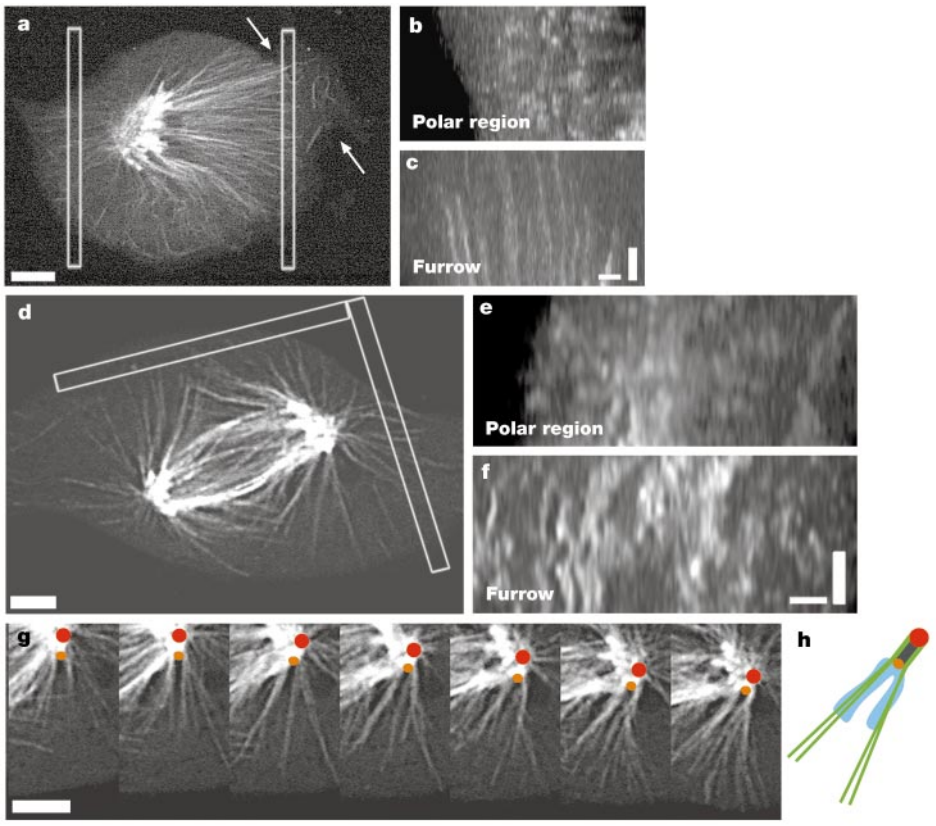

Figure 3 Chromosome-associated stable microtubules at the furrow. **a**, **d**, Live imaging of labelled tubulin in monopolar spindles (**a**) and untreated bipolar spindles (**d**) during anaphase. White rectangles roughly indicate source for kymographs. **b**, **c**, **e**, **f**, Kymograph of microtubules in the polar region (**b**, **e**) and furrow (**c**, **f**) used to analyse microtubule stability. **g**, Close-up view showing stable microtubules associated with the kinetochore fibres at their minus ends. Red circles mark the end of the kinetochore fibre. Orange circles mark the kinetochore. **h**, Schematic drawing of **g**. Horizontal scale bars, 5 μm; vertical scale bars, 400 s.

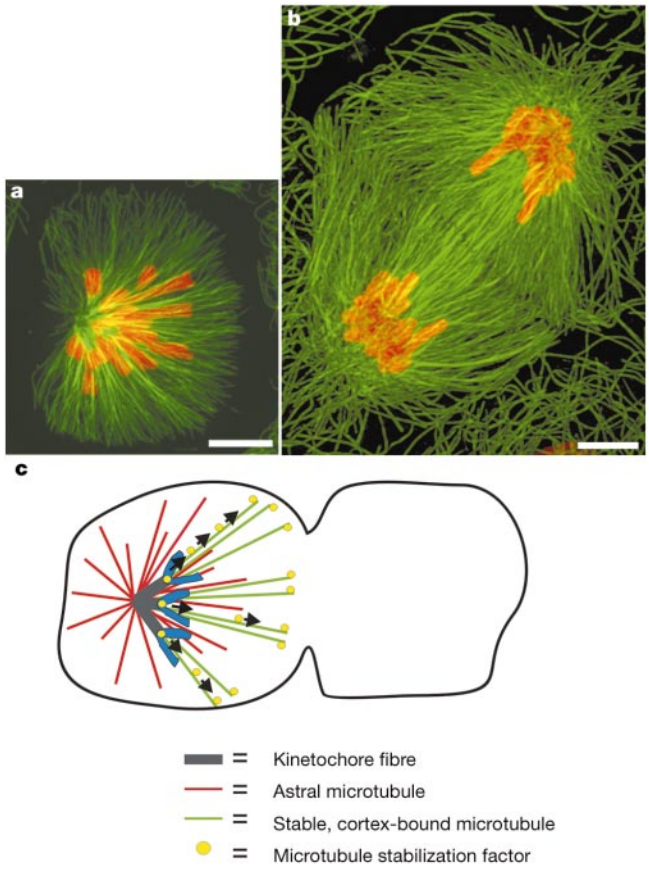

Figure 4 Model of cytokinesis induced by monopolar spindles. **a**, **b**, Normal bipolar microtubule array (**b**) is the sum of two, oppositely oriented, cytokinesis-inducing monopolar spindles (**a**). **c**, Centromere-bound microtubule stabilization factors are transported to the flanking microtubules on anaphase onset.

steep gradient of high numbers of stable microtubules flanking a region of low microtubule density is essential for furrow formation[4]. Models of how microtubules produce a non-uniform distribution of the cleavage stimulus during cytokinesis have previously relied on a difference in the numbers of microtubules in the polar versus the equatorial regions of the cell (for example, see refs 1–3, 4, 19, 20). Our observations suggest instead that a variation in microtubule dynamics in different regions of the cell is responsible for positioning the cell division plane. Specifically, chromosome-associated stable microtubules stimulate contractility in the cell equator. In addition, our data concur with the possibility that non-chromosome-associated dynamic microtubules may prevent ectopic furrowing in the polar regions of the cell, as would occur in the absence of microtubules[9,17,18].

In motile cells, differential microtubule dynamics seem to control the actin cytoskeleton differentially. That is, dynamic microtubules at the leading edge of the cell promote actin-dependent cell protrusion and stable microtubules at the cell rear promote actin-dependent cell tail retraction[21]. We propose that a similar asymmetry in microtubule dynamics leads to non-uniformity of a cleavage stimulus resulting in cytokinesis. We have constructed a model of cytokinesis in cultured cells in which microtubules associated with chromosomes or centromeres form persistent associations with the cell cortex through the transport of centromere-bound microtubule stabilization factors, of yet unknown identity, to the plus ends of these microtubules (Fig. 4c). These stable microtubules trigger the cell cortex to become contractile, forming a productive furrow in their vicinity. At the same time, the dynamic microtubules in the polar regions are probably acting to suppress ectopic furrowing outside the cell equator. This model would explain the furrowing pattern seen in *Sciara coprophilia* monopolar meiosis[22] and cellularizing syncitial *Drosophila melanogaster* embryos[23], and may be important for generating cells without nuclei, such as platelets[24]. □

Methods

Tissue culture, drug treatment, and anaphase induction

Monastrol was used at a concentration of 100 μM in either F-12 medium (Sigma) for pretreatment or phenol-red-free L-15 medium (Sigma) for filming. Pretreatments were done for at least 1 h, but up to 6 h, before imaging. We cultured, injected and imaged PtK1 cells as described[9]. His-tagged Mad2ΔC and glutathione *S*-transferase (GST)-tagged Mad1F10 were used to induce precocious anaphase as described[11,12].

Injection and filming chambers

Mitotic PtK1 cells were injected with tubulin labelled with X-rhodamine either alone or together with X-phalloidin labelled with Alexa 488 at room temperature to maintain the cells in mitosis throughout the injections. All filming was done at 37 °C as described[25]. For imaging tubulin, we used a needle concentration of 1 μM tubulin. Chambers were prepared[25] using phenol-red-free L-15 (Gibco-BRL) supplemented with Oxyrase (Oxyrase Inc.) to minimize photobleaching.

Live-cell imaging

Stage temperature was maintained at about 35–37 °C using an ASI 400 air curtain incubator (Nevtek). Images were taken at intervals of 15–20 s with an UltraVIEW spinning disc confocal scanning head (Perkin-Elmer) on a TE300 microscope (Nikon) using an Orca I, Orca II or Orca ER camera (Hamamatsu Photonics). These images were then digitally processed to enhance the contrast, using Metamorph imaging software (Universal Imaging).

Kinetochore fibre and chromosome identification

Kinetochore fibres were identified as the small bright bundles of microtubules terminating at a chromosome with the kinetochore at the site of the chromosome/kinetochore fibre interface. Chromosomes were easily identifiable because they excluded the free labelled tubulin that filled the remainder of the cell.

Cortex interaction measurements

Custom alignment and rotation algorithms in MetaMorph were used to correct for spindle and/or cell rotation. Aligned sequences were analysed by kymographs. In brief, a region of interest within the sequence (that is, the equatorial region of the cortex) was cropped and entered into the three-dimensional reconstruction algorithm in MetaMorph and a single '90°' view through the stack was generated. The resulting image was a two-dimensional representation of the time-lapse movie, in which time was the y dimension and positions over time of all the microtubules in this region appeared as lines parallel with the y axis. We obtained lifetimes of microtubules in the selected region by measuring the length of the lines in the kymograph images. Statistical analysis was done in Excel (Microsoft).

Received 31 January; accepted 9 June 2003; doi:10.1038/nature01860.
Published online 6 August 2003.

1. Rappaport, R. *Cytokinesis in Animal Cells* (Cambridge Univ, Cambridge, UK, 1997).
2. Harris, A. K. & Gewalt, S. L. Simulation testing of mechanisms for inducing the formation of the contractile ring in cytokinesis. *J. Cell Biol.* **109,** 2215–2223 (1989).
3. White, J. G. & Borisy, G. G. On the mechanism of cytokinesis in animal cells. *J. Theor. Biol.* **101,** 289–316 (1983).
4. Mandato, C. A., Benink, H. A. & Bement, W. M. Microtubule–actomyosin interactions in cortical flow and cytokinesis. *Cell Motil. Cytoskeleton* **45,** 87–92 (2000).
5. Wolf, N., Hirsh, D. & McIntosh, J. R. Spermatogenesis in males of the free-living nematode, *Caenorhabditis elegans*. *J. Ultrastruct. Res.* **63,** 155–169 (1978).
6. Rappaport, R. Experiments concerning the cleavage stimulus in sand dollar eggs. *J. Exp. Zool.* **148,** 81–89 (1961).
7. Mayer, T. U. *et al.* Small molecule inhibitor of mitotic spindle bipolarity identified in a phenotype-based screen. *Science* **286,** 971–974 (1999).
8. Kapoor, T. M., Mayer, T. U., Coughlin, M. L. & Mitchison, T. J. Probing spindle assembly mechanisms with monastrol, a small molecule inhibitor of the mitotic kinesin, Eg5. *J. Cell Biol.* **150,** 975–988 (2000).
9. Canman, J. C., Hoffman, D. B. & Salmon, E. D. The role of pre- and post-anaphase microtubules in the cytokinesis phase of the cell cycle. *Curr. Biol.* **10,** 611–614 (2000).
10. Gorbsky, G. J., Chen, R. H. & Murray, A. W. Microinjection of antibody to Mad2 protein into mammalian cells in mitosis induces premature anaphase. *J. Cell Biol.* **141,** 1193–1205 (1998).
11. Canman, J. C., Salmon, E. D. & Fang, G. Inducing precocious anaphase in cultured mammalian cells. *Cell Motil. Cytoskeleton* **52,** 61–65 (2002).
12. Canman, J. C. *et al.* Anaphase onset does not require the microtubule-dependent depletion of kinetochore and centromere-binding proteins. *J. Cell Sci.* **115,** 3787–3795 (2002).
13. Wheatley, S. P., Kandels-Lewis, S. E., Adams, R. R., Ainsztein, A. M. & Earnshaw, W. C. INCENP binds directly to tubulin and requires dynamic microtubules to target to the cleavage furrow. *Exp. Cell Res.* **262,** 122–127 (2001).
14. Murata-Hori, M. & Wang, Y. L. Both midzone and astral microtubules are involved in the delivery of cytokinesis signals: insights from the mobility of aurora B. *J. Cell Biol.* **159,** 45–53 (2002).
15. Adams, R. R., Carmena, M. & Earnshaw, W. C. Chromosomal passengers and the (aurora) ABCs of mitosis. *Trends Cell Biol.* **11,** 49–54 (2001).
16. Mackay, A. M., Ainsztein, A. M., Eckley, D. M. & Earnshaw, W. C. A dominant mutant of inner

centromere protein (INCENP), a chromosomal protein, disrupts prometaphase congression and cytokinesis. *J. Cell Biol.* **140,** 991–1002 (1998).
17. Shannon, K. B., Canman, J. C. & Salmon, E. D. Mad2 and BubR1 function in a single checkpoint pathway that responds to a loss of tension. *Mol. Biol. Cell* **13,** 3706–3719 (2002).
18. Kurz, T. *et al.* Cytoskeletal regulation by the Nedd8 ubiquitin-like protein modification pathway. *Science* **295,** 1294–1298 (2002).
19. Dechant, R. & Glotzer, M. Centrosome separation and central spindle assembly act in redundant pathways that regulate microtubule density and trigger cleavage furrow formation. *Dev. Cell* **4,** 333–344 (2003).
20. Asnes, C. F. & Schroeder, T. E. Cell cleavage. Ultrastructural evidence against equatorial stimulation by aster microtubules. *Exp. Cell Res.* **122,** 327–338 (1979).
21. Wittmann, T. & Waterman-Storer, C. M. Cell motility: can Rho GTPases and microtubules point the way? *J. Cell Sci.* **114,** 3795–3803 (2001).
22. Kubai, D. F. Meiosis in *Sciara coprophila*: structure of the spindle and chromosome behavior during the first meiotic division. *J. Cell Biol.* **93,** 655–669 (1982).
23. Foe, V. E., Field, C. M. & Odell, G. M. Microtubules and mitotic cycle phase modulate spatiotemporal distributions of F-actin and myosin II in *Drosophila* syncytial blastoderm embryos. *Development* **127,** 1767–1787 (2000).
24. Radley, J. M. & Scurfield, G. The mechanism of platelet release. *Blood* **56,** 996–999 (1980).
25. Howell, B. J., Hoffman, D. B., Fang, G., Murray, A. W. & Salmon, E. D. Visualization of Mad2 dynamics at kinetochores, along spindle fibres, and at spindle poles in living cells. *J. Cell Biol.* **150,** 1233–1250 (2000).

Supplementary Information accompanies the paper on **www.nature.com/nature**.

Acknowledgements We thank B. Bowerman, J. Sekelsky, N. Salmon, A. Harris and K. Bloom for comments on the manuscript; C. Waterman-Storer for discussions; the Cell Division Group at the Marine Biological Laboratory in Woods Hole; and B. Howell, D. Cimini, J. DeLuca, K. Shannon, C. Pearson, B. Moree and all members of the Salmon laboratory for support.

Competing interests statement The authors declare that they have no competing financial interests.

Correspondence and requests for materials should be addressed to E.D.S. (tsalmon@email.unc.edu).

S-phase checkpoint proteins Tof1 and Mrc1 form a stable replication-pausing complex

Yuki Katou[1,2], Yutaka Kanoh[1,2], Masashige Bando[1], Hideki Noguchi[1], Hirokazu Tanaka[1,3], Toshihiko Ashikari[4] & Katsunori Sugimoto[5] Katsuhiko Shirahige[1]

[1]*Genome Structure and Function Team, Human Genome Research Group, RIKEN Genomic Science Center, 1-7-22 Suehiro-cho, and* [2]*Science of Biological Supramolecular Systems, Graduate School of Integrated Science, Yokohama City University, 1-7-29 Suehiro-cho, Tsurumi-ku, Yokohama, Kanagawa, 230-0045, Japan*
[3]*Division of Biochemistry, Kihara Institute for Biological Research and Graduate School of Integrated Science, Yokohama City University, 641-12, Maioka-cho, Totsuka-ku, Yokohama, Kanagawa, 244-0813, Japan*
[4]*Institute for Advanced Technology, Suntory Limited, 1-1-1, Wakayamadai, Shimamoto-cho, Mishima-gun, Osaka, 618-8503, Japan*
[5]*Division of Biological Science, Nagoya University Graduate School of Science, Nagoya, 464-0814, Japan*

The checkpoint regulatory mechanism has an important role in maintaining the integrity of the genome[1–5]. This is particularly important in S phase of the cell cycle, when genomic DNA is most susceptible to various environmental hazards[3,6,7]. When chemical agents damage DNA, activation of checkpoint signalling pathways results in a temporary cessation of DNA replication. A replication-pausing complex is believed to be created at the arrested forks to activate further checkpoint cascades, leading to repair of the damaged DNA. Thus, checkpoint factors are thought to act not only to arrest replication but also to maintain a stable replication complex at replication forks[6–9]. However, the molecular mechanism coupling checkpoint regulation and replication arrest is unknown. Here we demonstrate that the checkpoint regulatory proteins Tof1 and Mrc1 interact directly with the DNA replication machinery in *Saccharomyces cerevisiae*. When hydroxyurea blocks chromosomal replication, this assembly forms a stable pausing structure that serves to anchor subsequent DNA repair events.

We developed a high-density oligonucleotide array that was able to analyse yeast chromosome VI at a 300-base pair (bp) resolution, in order to understand the interaction of checkpoint factors with the DNA replication machinery. A total of 13,982 oligonucleotides (25-base nucleotides) were designed to cover the entire length (270 kilobases (kb)) of the chromosome. In a log-phase culture we demonstrated the detection of Orc1, a subunit of the origin recognition complex, bound to every known origin on chromosome VI (refs 10, 11; Fig. 1a). This shows that our chromatin immunoprecipitation (ChIP)-chip method[12,13] can detect protein-binding sites at a resolution of at least 600 bp. In the following analyses, we used cells that were arrested at the G1 phase by α-factor, and then released into S phase in the presence of 200 mM hydroxyurea (HU) to activate replication checkpoint. Under these conditions we analysed the location of Cdc45, a protein involved in initiation and elongation steps of chromosomal DNA replication, and Pol1, a subunit of DNA polymerase α (Fig. 1b). Both showed localization only to early replicating regions, near autonomously replicating sequences (ARS) 607, 606, 605 and 603.5, suggesting that our ChIP–chip method can monitor locations of two proteins simultaneously. To analyse dynamic aspects of replication-related proteins during replication, we determined replicated regions by 5-bromodeoxyuridine (BrdU) incorporation simultaneously with protein binding. We used a yeast strain engineered to take up BrdU efficiently[14] to detect BrdU incorporation on the chip simultaneously with the location of Cdc45 (Fig. 1c). Locations of BrdU incorporation coincided clearly with Cdc45 binding. The replicated regions determined by BrdU incorporation in the presence of 200 mM HU were consistent with data obtained by quantitative polymerase chain reaction using a wild-type strain (data not shown).

Next, we determined the location of components involved in the S-phase checkpoint signal cascade (Ddc1, Mec3, Ddc2, Tof1, Mrc1, Rad9, Rad24 and Rad53 (refs 1, 2)) through challenge with 200 mM HU at S phase (Fig. 1d; see also Supplementary Fig. S1). We could not detect any significant signals for Rad9, and association of Rad24 was detected mainly near telomeres. We could not detect the association of Rad53 under these conditions; however, when we used DMA (dimethyl adipimidate)—a protein–protein crosslinking reagent[15]—before formaldehyde fixation, Rad53 association with replicating regions became barely detectable (Supplementary Fig. S1). Locations of all other checkpoint proteins overlapped with BrdU incorporation, suggesting that either these proteins moved together with replication forks, or that they were recruited to stalled forks in search of specific DNA structures. To address this question, protein-binding patterns during early replication in the absence of HU was determined. Cells were released from G1 arrest at low temperature (16 °C) in the medium without HU to slow the DNA synthesis, and collected every 10 min to analyse locations of Tof1, Pol1 (Fig. 2a, b) Ddc1, Ddc2 and Mrc1 (Supplementary Fig. S2). Tof1, Mrc1 and Pol1 localized to early replication origins, and moved away from replication origins as time passed. Co-localization of Tof1 or Mrc1 with Pol1 was estimated by the correlation coefficient of their patterns of localization for each time point. They were 0.70 (40 min), 0.79 (50 min) and 0.78 (60 min) between Pol1 and Tof1 localization, and 0.43 (40 min), 0.70 (50 min) and 0.89 (60 min) between Pol1 and Mrc1 localization. This suggests that Tof1 and Mrc1 are located in replication forks as components of the replication machinery during normal S-phase progression. Not all of the components of the S-phase

